Appl. Phys. A 50, 385–396 (1990)

Applied Physics A Solids and Surfaces

On the Reaction Kinetics in Laser-Induced Pyrolytic Chemical Processing

D. Bäuerle, B. Luk'yanchuk*, and K. Piglmayer

Angewandte Physik, Johannes-Kepler-Universität Linz, A-4040 Linz, Austria

Received 11 September 1989/Accepted 2 November 1989

Abstract. Reaction rates, particle densities, and temperature distribution in pyrolytic (photothermal) laser-induced microchemical processing are investigated with respect to temperature and concentration-dependent transport coefficients, and with respect to the effect of thermal diffusion. While the model employed is particularly suitable for laser-induced chemical vapor deposition (LCVD), it can also be applied to many cases of laser-induced surface modification and dry-etching.

PACS: 42.5, 68, 82.65

The reaction rates achieved in laser chemical processing (LCP) are of great relevance to both the applications of the technique and the elucidation of the fundamental microscopic mechanisms involved [1]. In the latter connection the analysis of experimental data on the basis of model calculations has been found extremely useful [2]. In pyrolytic (photothermal) LCP the analysis of reaction rates requires a knowledge of both the laser-induced temperature rise on the substrate to be processed, and of the transport phenomena within the ambient medium. While direct measurements of the local laser-induced temperature rise have actually been demonstrated in a few exceptional cases, the information on the material transport is almost exclusively based on model calculations.

In this paper we report on theoretical investigations on transport phenomena in pyrolytic laser-induced chemical processing. In contrast to earlier investigations [2], the present calculations take into account temperature and concentration-dependences of the transport coefficients, and also consider the effect of thermal diffusion. While the model employed is particularly appropriate to pyrolytic laser-induced chemical vapor deposition (LCVD), it can be applied to many cases of pyrolytic laser-induced surface modification (surface oxidation, reduction, doping, etc.) and etching. Furthermore, some of the equations are formulated in such a general way that they can be adapted to certain cases of pyrolytic LCP from liquid-like phases.

The paper is organized as follows: The model and the various different assumptions employed in the calculations are presented in Sect. 1. In Sect. 2 the kinetics of pyrolytic LCP is investigated with respect to the temperature dependences in the particle density, the molecular diffusion coefficient, and the thermal conductivity. The effect of the concentration dependence of the thermal conductivity is studied in Sect. 3. In Sect. 4 the influence of thermal diffusion on the reaction rate is investigated. The most important results are summarized in Sect. 5.

1. Model

The experimental situation considered throughout this paper is depicted in Fig. 1. The reaction zone is described by a hemisphere of radius $r_D = d/2$ which is placed on a semiinfinite substrate. Henceforth, we assume *spherical symmetry* with respect to the center of this reaction zone. This geometry applies, for example, to laser-induced deposition of spots. The temperature on the surface $r = r_D$ shall be uniform and given by

$$T_S = T(\infty) + \Delta T_S, \tag{1}$$

where $T(\infty) \equiv T(r \to \infty)$ is the temperature far away from the reaction zone, and ΔT_S is the laser-induced

* On leave from: General Physics Institute, Academy of Sciences, SU-117942 Moscow, USSR

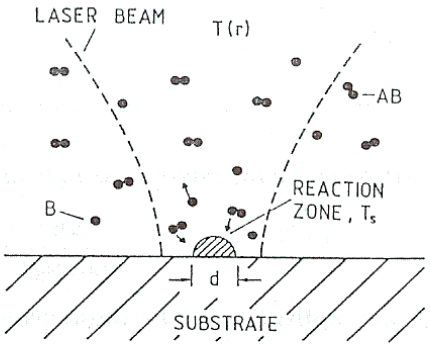

Fig. 1. Schematic for pyrolytic laser-induced chemical processing. The reaction zone is represented by a hemisphere of radius $r_D = d/2$ whose surface temperature, T_S, is uniform. The temperature of the ambient medium is $T(r)$. The origin of the radius vector, r, is in the center of the hemisphere. The laser radiation is exclusively absorbed on the surface $r = r_D$. Carrier gas or solvent molecules which may be present are not indicated

temperature rise on the surface r_D. We assume that T_S is not influenced by the heat of reaction and we also disregard any temperature jump at the interface between the solid and the ambient medium. Because of the latter assumption, we have $T_S = T(r_D)$ where $T(r_D)$ is the temperature of the ambient *at* the surface $r = r_D$. This approximation holds as long as r_D is much larger than the mean free path of molecules, λ_m. Typical temperature ranges investigated in LCP are $300\,K \leqq T_S \leqq 3500\,K$.

We now consider a photothermally activated reaction of the type

$$AB_\nu + G \rightarrow A(\downarrow) + \nu \cdot B(\uparrow) + G\,, \tag{2}$$

where AB_ν is the reactant and G either a carrier gas or, in the case of liquid-phase processing, a solvent. The reaction (2) shall be purely heterogeneous, i.e. the decomposition of AB_ν into A and B occurs exclusively on the surface $r = r_D$. The species A condense on this surface and either form the deposit or else react further, while the species B desorb directly. The decomposition of AB_ν according to (2) shall be of first order. Henceforth, we consider *stationary* conditions only. Therefore, the reaction rate W is independent of time and is given by

$$W = kN_{AB}(r_D) = kN(r_D)x_{AB}(r_D)\,, \tag{3}$$

where k is the rate constant, $N_{AB}(r_D)$ the particle density of species AB_ν at $r = r_D$, $N(r_D)$ the total particle density, and $x_{AB}(r_D)$ the molar ratio of species AB_ν. The molar ratio of species i is defined by $x_i = N_i/N$ with $\Sigma x_i = 1$. The rate constant is given by the Arrhenius law

$$k \equiv k(T_S) = k_0 \exp\left(-\frac{\Delta E}{k_B T_S}\right), \tag{4}$$

where ΔE is the apparent chemical activation energy, and k_B the Boltzmann constant. Subsequently we assume that the *total* number of particles per unit volume, N, shall remain unchanged by the reaction (2). In other words, we concentrate on *equimolecular* reactions where $\nu = 1$. Therefore, N will change only via the temperature distribution within the ambient medium, $T(r)$. Henceforth we define the particle density of species i at the coordinate r by $N_i(r) \equiv N_i(T(r))$. The total particle density is

$$N(r) = N_{AB}(r) + N_B(r) + N_G(r)\,. \tag{5}$$

We will consider cases with either $N_G = 0$ or $N_G \neq 0$. If $N_G = 0$, the $N_{AB}(\infty)$ will be large compared to $N_B(\infty)$, i.e. $N_{AB}(\infty) \gg N_B(\infty)$. If $N_G \neq 0$ we shall have $N_G \gg N_{AB}$. We assume that $N(r)$ is given by the equation of state

$$N(r) = N(\infty)\left(\frac{T(\infty)}{T(r)}\right)^q, \tag{6}$$

where, in the case of ideal gases, $q = 1$. We also investigate the case where the density N is *independent* of temperature. This approximation is characteristic for liquids and can be described by $q = 0$.

Furthermore, we choose conditions where the species AB, B, and G do *not* absorb the laser radiation. As a consequence, heating of the ambient medium originates only via the energy flux from the laser-heated surface $r = r_D$ into this medium. Here, we consider the energy transport by heat diffusion only. Transport by thermal radiation and by convection are disregarded. The preceding assumptions are self-consistent. Nevertheless, to disregard convection is certainly a very crude approximation if we are dealing with a high-density ambient medium, i.e. with high gas pressures or with liquids. However, in such cases the effect of convection can sometimes be estimated when the thermal conductivity κ and the molecular diffusion coefficient D, are replaced by other phenomenological parameters, κ' and D', that contain – besides κ and D – the convective terms κ_c and D_c, respectively [3]. In spite of these difficulties, we will henceforth term media that are described by the equation of state (6) with $q = 0$, as "liquids".

In order to permit a direct comparison between the various results presented in the following sections, we often introduce normalized quantities. The normalized radius is defined by

$$r^* = r/r_D \tag{7}$$

The normalized temperatures within the ambient medium, T^*, and at the surface of the reaction zone, T_S^*, are

$$\begin{aligned} T^*(r^*) &= T(r^*)/T(\infty)\,, \\ T_S^* &\equiv T^*(1) = T_S/T(\infty)\,, \\ \Delta T_S^* &\equiv \Delta T^*(1) = T_S^* - 1\,. \end{aligned} \tag{8}$$

The normalized apparent chemical activation energy is

$$\Delta E^* = \frac{\Delta E}{k_B T(\infty)}. \tag{9}$$

The normalized particle densities can be written as

$$\begin{aligned} N^*(r^*) &= \frac{N(r^*)}{N(\infty)}, \\ N_i^*(r^*) &= \frac{N_i(r^*)}{N_i(\infty)} = \frac{N(r^*)\cdot x_i(r^*)}{N(\infty)\cdot x_i(\infty)} \\ &= \frac{x_i^*(r^*)}{T^{*q}(r^*)}, \end{aligned} \tag{10}$$

where we have employed (6), and also introduced the normalized molar ratio

$$x_i^*(r^*) = \frac{x_i(r^*)}{x_i(\infty)}.$$

The normalized reaction rate is defined by

$$\begin{aligned} W^* &= \frac{W}{k_0 N(\infty) x_{AB}(\infty)} = \frac{k N(r_D) x_{AB}(r_D)}{k_0 N(\infty) x_{AB}(\infty)} \\ &= N^*(1) x_{AB}^*(1) \exp\left(-\frac{\Delta E^*}{T_S^*}\right). \end{aligned} \tag{11}$$

We also introduce the quantity

$$\varepsilon^* = \frac{k_0 r_D}{D_{AB}(\infty)} \tag{12}$$

which describes the influence of the size of the reaction zone, and of the molecular diffusion coefficient far away from this zone.

2. Temperature Dependences

In this section we investigate the reaction kinetics with respect to the temperature dependences of the particle density, the molecular diffusion coefficient, and the thermal conductivity. To this end the equation of continuity must be solved together with the heat equation and appropriate boundary conditions. With equimolecular reactions, the fluxes of species AB, j_{AB}, and of B, j_B, are related by $j_B = -j_{AB}$. The equation of continuity for species AB can then be written in the form

$$-\nabla j_{AB}(r) = \frac{1}{r^2}\cdot\nabla[r^2 N(r) D_{AB}(r)\cdot\nabla x_{AB}(r)] = 0, \tag{13}$$

where D_{AB} is the *effective* diffusion coefficient describing the diffusion of AB within the mixture. Because of the temperature distribution within the ambient medium, $T = T(r)$, *all* of the quantities depend on the coordinate r. The boundary conditions to (13) are

$$x_{AB}(r\to\infty) = x_{AB}(\infty) \tag{14}$$

and

$$\begin{aligned} -j_{AB}(r_D) &= N(r_D) D_{AB}(r_D)\left[\frac{\partial x_{AB}(r)}{\partial r}\right]_{r_D} \\ &= W = k N(r_D) x_{AB}(r_D). \end{aligned} \tag{15}$$

The latter condition means that the (net) reaction flux at the surface, $j_{AB}(r_D)$, is balanced by the reaction rate, W. The heat equation can be written in the form

$$\nabla[r^2\kappa(r)\nabla T(r)] = 0 \tag{16}$$

where κ is the thermal conductivity of the *mixture*. In (16) we have assumed that the molecular heat capacities c_p are equal with all species. The boundary conditions to (16) are

$$T(r = r_D) = T_S \tag{17}$$

and

$$T(r\to\infty) = T(\infty). \tag{18}$$

The solution of (13–18) yields for the molar ratio

$$x_{AB}(r) = x_{AB}(\infty)\left(1 - \frac{F(r)}{\zeta + F(r_D)}\right) \tag{19}$$

with

$$\zeta = \frac{D_{AB}(r_D)}{k r_D} = \frac{1}{\varepsilon^*}\exp\left(\frac{\Delta E}{k_B T_S}\right) \tag{20}$$

and

$$F(r) = r_D \cdot N(r_D) D_{AB}(r_D)\cdot\int_r^\infty \frac{dr'}{r'^2 f(r')} \tag{21}$$

with

$$f(r') = N(r')\cdot D_{AB}(r'). \tag{22}$$

The solution for the temperature distribution within the ambient medium is

$$T(r) = T(\infty) + \Delta T_S \cdot \Phi(r) \tag{23}$$

with

$$\Phi(r) = \int_r^\infty \frac{dr'}{r'^2\kappa(r')}\cdot\left(\int_{r_D}^\infty \frac{dr'}{r'^2\kappa(r')}\right)^{-1} \tag{24}$$

if κ is *independent* of temperature, (24) simply yields $\Phi(r) = r_D/r$.

For the case of gases we employ temperature dependences of the transport coefficients as given in [4]

$$D_i(r) = D_i(\infty)\left(\frac{T_G(r)}{T_G(\infty)}\right)^n = D_i(\infty) T_G^{*n}(r) \tag{25a}$$

and

$$\kappa(r) = \kappa(\infty)\left(\frac{T_G(r)}{T_G(\infty)}\right)^m = \kappa(\infty) T_G^{*m}(r) \tag{26}$$

where T_G is the gas-phase temperature. Within the framework of the kinetic theory of gases [4], the exponents are within the ranges $1.5 \leqq n \leqq 2$ and $0.5 \leqq m \leqq 1.5$.

In the case of liquids, the thermal conductivity can also be described, in good approximation, by (26). The temperature dependence of the molecular diffusion coefficient, however, is more complicated. In the phenomenological theory of liquids it is described by [4]

$$D_i(r) = D_i(\infty)\frac{T_L(r)}{T_L(\infty)}\exp\left(-\frac{\Delta E}{k_B T_L(r)}\right) = D_i(\infty)T_L^*(r)\exp\left(-\frac{\Delta E^*}{T_L^*(r)}\right), \quad (25b)$$

where $T_L(r)$ is the temperature distribution within the liquid. For small temperature intervals, however, (25b) may be approximated by (25a) where the value of n is then within ranges $1 \leqq n \leqq 10$.

In order to permit a wide application of the present theory, the subsequent calculations are performed with arbitrary values of q, n, and m. With (6, 22, and 25a), Eq. (21) becomes

$$F(r) = r_D \cdot T_S^{n-q} \int_r^\infty \frac{dr'}{r'^2 T^{n-q}(r')}, \quad (27)$$

where $T(r)$ is the temperature within the gas or the liquid phase. Correspondingly, (23) together with (24) and (26) becomes

$$T^{m+1}(r) = T^{m+1}(\infty) + [T_S^{m+1} - T^{m+1}(\infty)]\cdot\frac{r_D}{r} \quad (28)$$

When normalized quantities are introduced, as defined in Sect. 1, the integration of (27), after substitution of (28), yields

$$F_{q,n,m}(r^*) = \left(\frac{m+1}{m+q-n+1}\right)\left(\frac{T_S^{*n-q}}{T_S^{*m+1}-1}\right) \times \left\{\left[1+(T_S^{*m+1}-1)\frac{1}{r^*}\right]^{\frac{m+q-n+1}{m+1}} - 1\right\} \quad (29a)$$

if $m+q-n+1 \neq 0$, and

$$F_{q,n,m}(r^*) = \frac{T_S^{*m+1}}{T_S^{*m+1}-1}\ln\left[1+(T_S^{*m+1}-1)\frac{1}{r^*}\right] \quad (29b)$$

if $m+q-n+1=0$.

Together with (25a) the molar ratio (19) can be rewritten in the form

$$x_{AB}^*(r^*) = 1 - \frac{\varepsilon^* F_{q,n,m}(r^*)\cdot T_S^{*-n}\cdot\exp(-\Delta E^*/T_S^*)}{1+\varepsilon^*\cdot F_{q,n,m}(1)\cdot T_S^{*-n}\cdot\exp(-\Delta E^*/T_S^*)}. \quad (30)$$

Correspondingly, the reaction rate (11) becomes

$$W^*(T_S^*) = \frac{T_S^{*-q}\cdot\exp(-\Delta E^*/T_S^*)}{1+\varepsilon^*\cdot F_{q,n,m}(1)\cdot T_S^{*-n}\cdot\exp(-\Delta E^*/T_S^*)}. \quad (31)$$

The temperature distribution within the ambient medium is

$$T^*(r^*) = \left[1+(T_S^{*m+1}-1)\frac{1}{r^*}\right]^{\frac{1}{m+1}}. \quad (32)$$

The preceding equations will be discussed in Sects. 2.1 and 2.2 for different equations of state, (6), characterized by $q=1$ and $q=0$, respectively.

2.1. Gas-Phase Processing ($q=1$)

The preceding formalism will now be applied to gas-phase processing where $q=1$. To demonstrate the relative importance of single dependences, we will discuss three different cases that are characterized by exponents $(q=1, n, m)$.

Case 1: $q=1$; $n=0$; $m=0$.

In this case, both the diffusion coefficient D_{AB} and the thermal conductivity κ are independent of temperature. The spatial distributions of the particle density $N_{AB}^*(r^*)$ and of the concentration $x_{AB}^*(r^*)$ are shown by *dashed* curves in Figs. 2 and 3, respectively.

In Fig. 2a parameter values $\Delta E^*=90$ and $\varepsilon^*=5\times10^6$ have been employed. These values are typical for the deposition of carbon from C_2H_2, and of Si from SiH_4 [1, 5]. In Fig. 2b the corresponding parameter values are $\Delta E^*=45$ and $\varepsilon^*=5\times10^4$. This parameter set is appropriate, for example, to pyrolytic LCVD of Ni from $Ni(CO_4)$ [1]. With both parameter sets, N_{AB}^* is much smaller than unity even with $r^*=5$, and it further decreases with decreasing values of r^*. With $T_S^*=10$ the particle density at the surface of the reaction zone ($r^*=1$) almost vanishes. This behavior is typical for mass transport limitation. Kinetic aspects become more evident from the concentration dependence $x_{AB}^*(r^*)$ that is plotted in Fig. 3 for the same parameter sets. The present case is again included in these figures by *dashed* curves. In Fig. 3a the $x_{AB}^*\approx1$ within the total region $1\leqq r^*\leqq5$ if $T_S^*=4$. With $T_S^*=10$, the $x_{AB}^*>0.9$ with $r^*\geqq5$ and it almost vanishes with $r^*\to1$. The behavior observed with surface temperatures $T_S^*=4$ and 10 is typical for reactions that are controlled by the chemical kinetics and by mass transport, respectively. With the parameter set employed in Fig. 3b, mass transport influences the reaction rate even with $T_S^*=4$.

The comparison of Figs. 2 and 3 shows that the overall decrease in particle density N_{AB}^* originates from gas-phase heating.

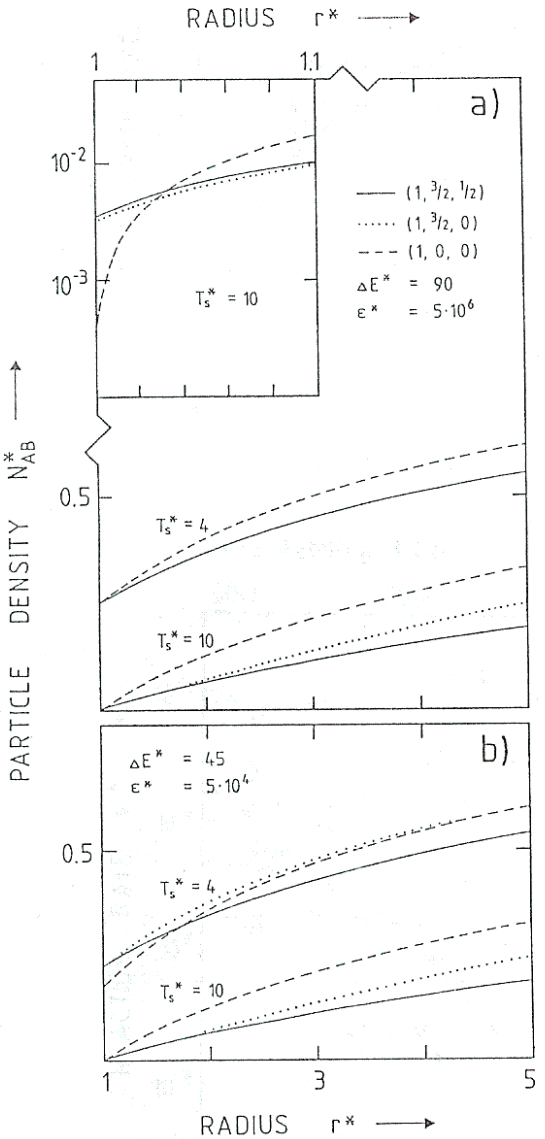

Fig. 2. Spatial distribution of normalized particle density $N_{AB}^*(r^*)$ of *gaseous* species AB for normalized substrate temperatures $T_S^*=4$, and 10. *Full* curves: Both the molecular diffusion coefficient D_{AB} and thermal conductivity κ depend on temperature ($q=1$, $n=3/2$, $m=1/2$). *Dotted* curves: D_{AB} temperature-dependent only ($q=1$, $n=3/2$, $m=0$). *Dashed* curves: D_{AB} and κ independent of temperature ($q=1, n=0, m=0$). **a** $\Delta E^*=90$, $\varepsilon^*=5\times10^6$. With $T_S^*=4$, dashed and dotted curves coincide. **b** $\Delta E^*=45$, $\varepsilon^*=5\times10^4$

Arrhenius plots of the normalized reaction rate W^* are shown in Fig. 4 for various parameter sets. The results that apply to the present case are again included in the figures by dashed curves. An increase in ε^* corresponds to either an increase in reaction zone radius r_D and/or to a decrease in the diffusion coefficient $D_{AB}(\infty)$, see (12). If we consider a reaction of the type (2) with $\nu=1$, $N_G=0$, and $N_{AB}\gg N_B$, the pressure dependence of the diffusion coefficient can be described by $D_{AB}\propto 1/p_{AB}(\infty)$. In this case the increase in ε^* can also be interpreted by an increase in the pressure $p_{AB}(\infty)$. If, on the other hand, $N_G\neq 0$ and $N_{AB}\ll N_G$, the total pressure can be approximated by $p=p_{AB}+p_G+p_B\approx p_G$. As a consequence, D_{AB} becomes independent of p_{AB} and can be described by $D_{AB}\propto 1/p_G$. With the decrease in activation energy (Fig. 4b) the reaction rate is transport limited within the whole temperature regime, except for values $\varepsilon^*\leqq 10^2$.

The distribution of the normalized gas-phase temperature $T_G^*(r^*)$ is shown in Fig. 5, also by *dashed* curves. According to (32) the temperature distribution depends only on the surface temperature T_S.

Case 2: $q=1$, $n=\frac{3}{2}$; $m=0$.

In this case we investigate the influence of a temperature dependent *diffusion* coefficient according to (25a). With $m=0$ the thermal conductivity is assumed to be a constant.

The spatial dependences of $N_{AB}^*(r^*)$ and of $x_{AB}^*(r^*)$ are included by *dotted* curves in Figs. 2 and 3, respectively. Within the kinetically controlled regime, i.e. with $T_S^*=4$ and the parameter set employed in Figs. 2a and 3a, the dotted curves coincide with the dashed curves within the total range $1\leqq r^*\leqq 5$. The situation is somewhat different in Figs. 2b and 3b (in Fig. 3b with $T_S^*=4$ the dotted curve coincides with the full curve). Here, with $T_S^*=4$ both the particle density and the concentration are increased with respect to case 1, in particular near the surface of the reaction zone. The situation is quite different with $T_S^*=10$. Here, the dotted curves are always *below* the dashed curves, except near the surface of the reaction zone, where both N_{AB}^* and x_{AB}^* are increased with respect to *Case 1* (see inset in Fig. 2a). The crossover between dashed and dotted curves occurs near $r^*\approx 1.03$. In other words, consideration of the temperature dependence of D_{AB} results in a *significant* increase in particle density N_{AB}^* and concentration x_{AB}^* at the surface $r^*=1$, and to a decrease of these quantities away from the reaction zone.

Arrhenius plots of the reaction rate W^* are included in Figs. 4a, b by dotted curves. It becomes evident that the increase in diffusion coefficient with temperature considerably increases the reaction rate within the transport limited regime. Clearly, the kinetically controlled regime remains unaffected.

The temperature distribution (32) depends on the exponent m only, and it is therefore identical to that of case 1.

Case 3: $q=1$; $n=\frac{3}{2}$; $m=\frac{1}{2}$.

This parameter set is most typical within the framework of the kinetic theory of gases [4].

The density $N_{AB}^*(r^*)$ and the concentration $x_{AB}^*(r^*)$ are included in Figs. 2 and 3 by *full* curves. The spatial

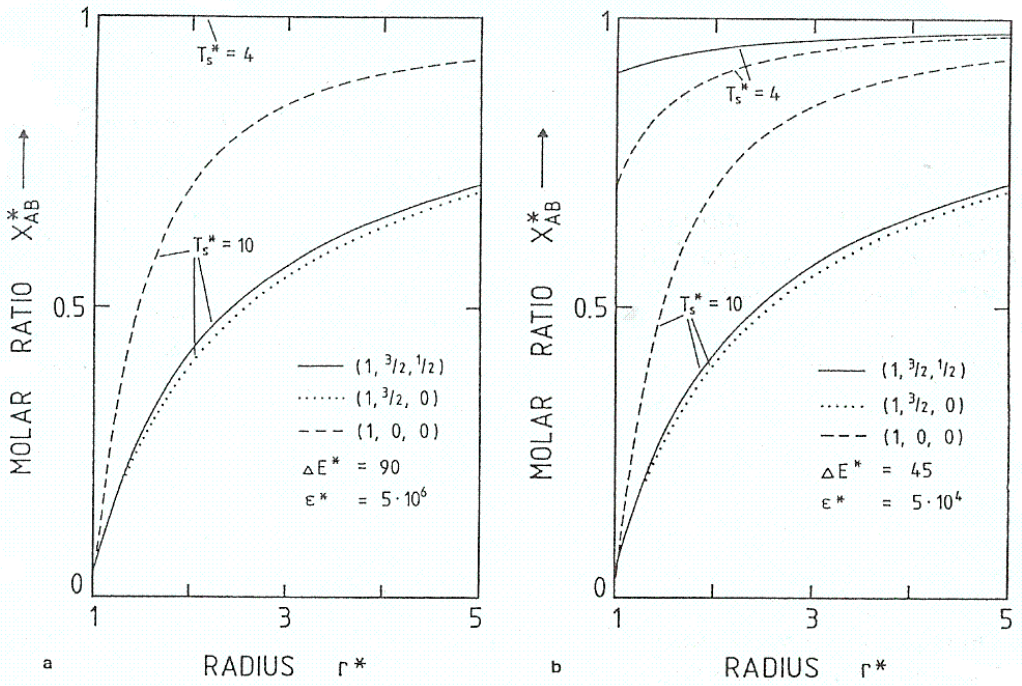

Fig. 3. Same as Fig. 2, but for the concentration x^*_{AB}. With $T_S^* = 4$ full and dotted curves coincide

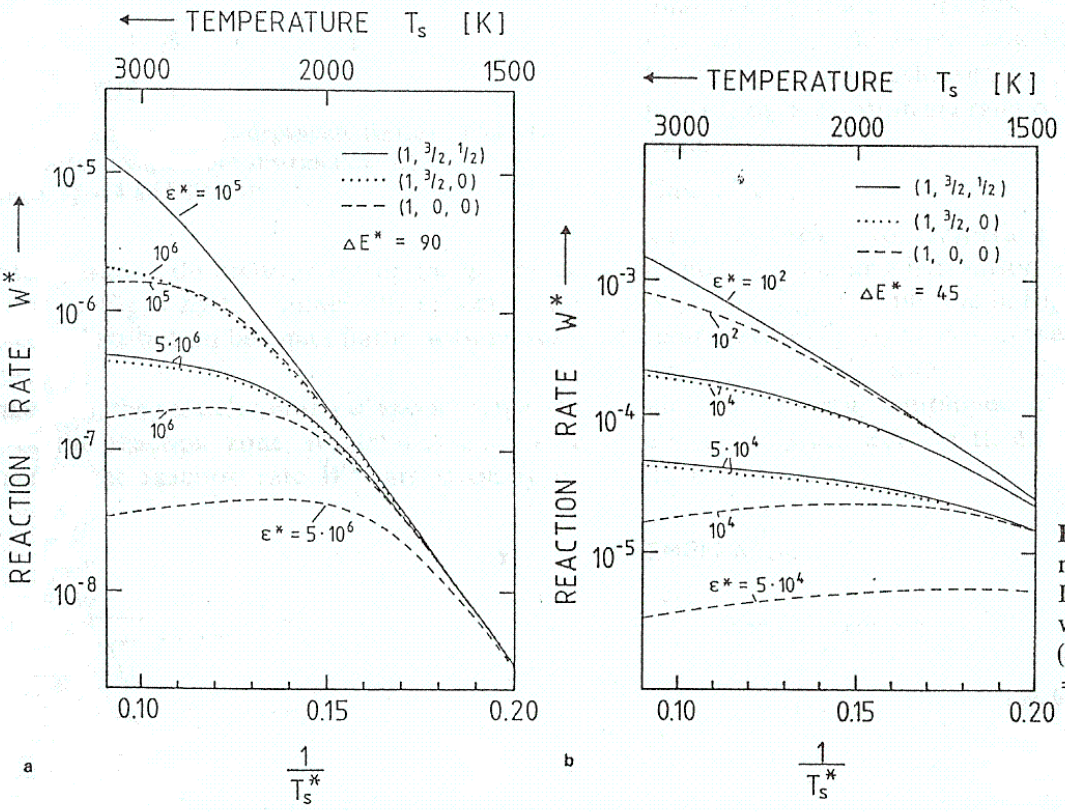

Fig. 4a, b. Arrhenius plots of normalized reaction rate W^*. Different curves belong to various values of ε^* and parameter sets $(q=1, n, m)$. **a** $\Delta E^*=90$; **b** $\Delta E^*=45$

dependence of the concentrations $x^*_{AB}(r^*)$ remains almost unaffected with respect to case 2 for all of the parameter sets investigated (compare full and dotted curves in Figs. 3a and b). This is different for the particle density N^*_{AB} which, for $r^*>1$, is diminished with respect to case 2 (compare full and dotted curves in Fig. 2). The decrease observed in $N^*_{AB}(r^*)$ is a consequence of the increase in gas-phase temperature (compare full and dashed curves in Fig. 5). In other words, the temperature dependence of κ decreases the concentration N^*_{AB} for distances $r^*>1$, but has almost no influence for $r^*=1$.

Arrhenius plots of the reaction rate are included in Figs. 4a, b by *full* curves. Comparison of full and dotted curves for the same values of ε^* shows that the temperature dependence of κ has only very limited influence on the reaction rate W^*. This is, of course, consistent with the results depicted in Fig. 2.

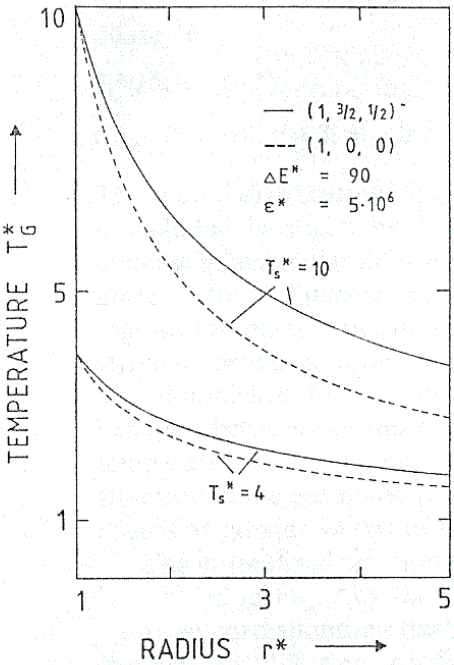

Fig. 5. Influence of temperature-dependent thermal conductivity on the gas-phase temperature distribution $T_G^*(r^*)$ for surface temperatures $T_S^*=4$ and $T_S^*=10$

The temperature distribution within the gas-phase is included in Fig. 5 by full curves. As expected, the temperature distribution becomes flatter with increasing values of κ.

In *summary*, the particle density of species AB at the surface of the reaction zone, $N_{AB}(r^*=1)$ and, as a consequence, the reaction rate W^*, are strongly influenced by the temperature dependence of the molecular diffusivity D_{AB}. On the other hand, the temperature dependence of the thermal conductivity has only very limited influence on these quantities.

2.2. *Liquid-Phase Processing* ($q=0$)

In this part we shall apply the preceding formalism to liquid-phase LCP. With the approximation $q=0$, we obtain from (10)

$$N_{AB}^*(r^*)=x_{AB}^*(r^*). \tag{33}$$

Subsequently, we will consider (30) to (32) for three sets of exponents ($q=0$, n, m). The main difference to gas-phase processing is the small temperature interval that can be investigated in liquid-phase processing, where T_S^* is, typically, between 1 and 2. The difficulty with quantitative calculations arises from the paucity of information on the kinetic constants k_0 and ΔE. From the reaction rates achieved in liquid-phase pyrolytic processing, activation energies of $\Delta E^*=10$ to 30 can be estimated [6].

Case 1: $q=0$, $n=0$, $m=0$.

This case refers to temperature-independent coefficients. The spatial distribution of the particle density $N_{AB}^*(r^*)=x_{AB}^*(r^*)$ is plotted in Fig. 6 for three substrate temperatures T_S^* by dashed curves. The parameters are $\Delta E^*=10$, $\varepsilon^*=10^3$, and $T_S^*=1.1$, 1.5, and 2. The small activation energy employed causes transport limitations to start even with the lowest temperature $T_S^*=1.1$.

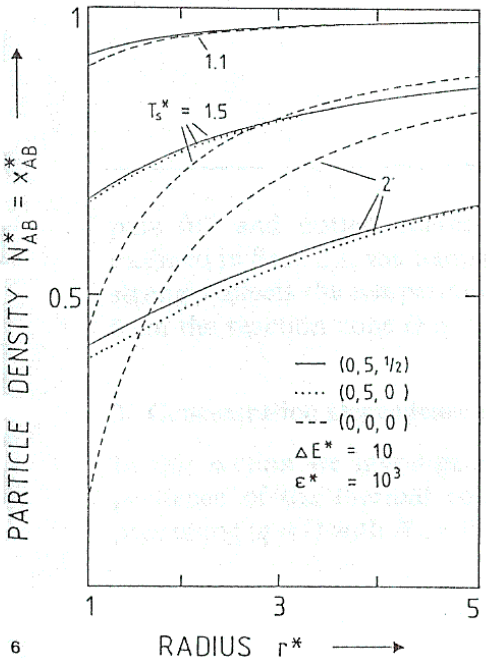

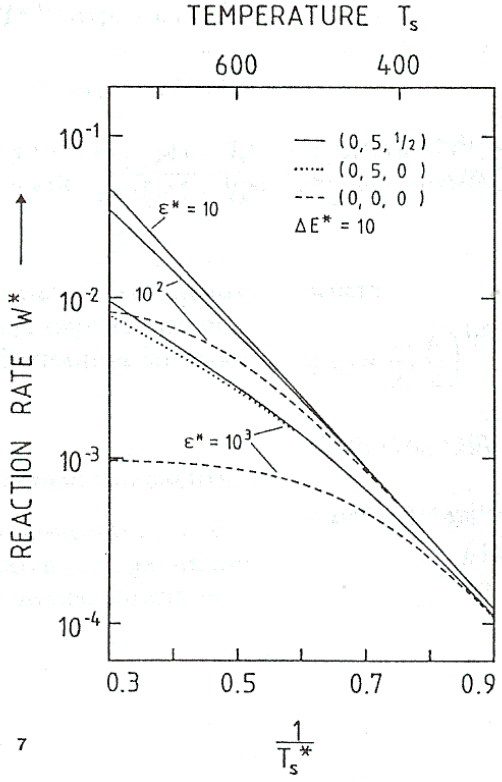

Fig. 6. Normalized density/concentration of species AB in the *liquid* phase for substrate-temperatures $T_S^*=1.1$, 1.5, and 2. The parameters employed were $\Delta E^*=10$ and $\varepsilon^*=10^3$. *Full curves:* $q=0$, $n=5$, $m=1/2$. *Dotted* curves: $q=0$, $n=5$, $m=0$. *Dashed* curves: $q=0$, $n=0$, $m=0$.

Fig. 7. Arrhenius plot of the normalized reaction rate in *liquid*-phase processing for $\Delta E^*=10$. Different curves belong to various values of ε^* and parameter sets ($q=0$, n m)

An Arrhenius plot of the normalized reaction rate is shown in Fig. 7 for $\Delta E^* = 10$ and for various values of ε^*. The *dashed* curves apply to the present case.

The temperature distribution (32) does not depend on q and n, and it is therefore equal to that in the gas phase i.e.

$$T_L^*(r^*) = T_G^*(r^*). \tag{34}$$

Case 2: $q=0$, $n=5$, $m=0$.

The spatial distribution $N_{AB}^*(r^*) = x_{AB}^*(r^*)$ for this case is included in Fig. 6 by dotted curves. Clearly, the increase in molecular diffusion coefficient with temperature only influences the mass-transport-limited regime. The particle density/concentration of species is strongly increased in the vicinity of the reaction zone, and diminished further away from this zone. This behavior becomes the more pronounced the higher the temperature T_S^*. In comparison to the corresponding situation in the gas phase (Figs. 2 and 3) the crossover occurs at greater values of r^*.

The normalized reaction rate for a value of $\varepsilon^* = 10^3$ is included in Fig. 7 by the *dotted* curve. Comparison with the corresponding dashed curve shows that the increase in diffusion coefficient with temperature almost eliminates the mass-transport limitation and causes a strong increase in the reaction rate within this region.

Case 3: $q=0$, $n=5$, $m=1/2$.

This case is included in Figs. 6 and 7 by the *solid* curves. As in the case of gas-phase processing, $N_{AB}^*(r^*)$, $x_{AB}^*(r^*)$ and W^* all remain almost unaffected by the temperature dependence of the thermal conductivity κ (compare full and dotted curves). However, as already outlined in Sect. 2.1, the temperature dependence of κ strongly affects the temperature distribution far away from the reaction zone (Fig. 5).

3. Concentration Dependence of Thermal Conductivity

In this section we investigate the concentration dependence of the thermal conductivity in gas-phase processing ($q=1$) with $N_G=0$. The molecular diffusivity of gases at low to medium pressures is, in good approximation, inversely proportional to the *total* gas pressure. It only depends very slightly, however, on the relative concentrations of the single gaseous components. We therefore use again the relation

$$D_{AB}(r^*) = D_{AB}(\infty) T_G^{*n}(r^*). \tag{35}$$

Henceforth, we set $n=3/2$. The concentration dependence of the thermal conductivity can be described by [4]

$$\kappa(x_{AB}, r^*) = [\kappa_{AB}(\infty) x_{AB}(r^*) + \kappa_B(\infty) x_B(r^*)] T_G^{*1/2}(r^*), \tag{36}$$

where $x_B = 1 - x_{AB}$. In (36) we have assumed the *same* temperature dependence for gases AB and B, i.e. $\kappa_i(r^*) = \kappa_i(\infty) \cdot T_G^{*1/2}(r^*)$. We now introduce the abbreviations

$$\bar{\kappa} = \tfrac{1}{2}[\kappa_{AB}(\infty) + \kappa_B(\infty)], \tag{37}$$

$$\Delta\kappa = \tfrac{1}{2}[\kappa_{AB}(\infty) - \kappa_B(\infty)]. \tag{38}$$

We can now rewrite (36) in the form

$$\kappa(x_{AB}, r^*) = [\bar{\kappa} - \Delta\kappa + 2\Delta\kappa x_{AB}(r^*)] T_G^{*1/2}(r^*), \tag{39}$$

From (13), (16), and (39) we obtain

$$T_G^{*1/2} r^{*2} \frac{d}{dr^*}\left[\frac{1}{r^{*2}} T_G^{*-1/2}\left(\frac{dT_G^*}{dr^*}\right)^{-1}\right] = -\mu \tag{40}$$

with

$$\mu = \frac{2\Delta\kappa}{\bar{\kappa}} C x_{AB}(\infty) = \text{const}, \tag{41}$$

where C is a constant that is determined from the boundary conditions. Integration of (40) yields

$$r^{*-1} = \frac{\int_1^{T_G^*} T_1^{*1/2} \exp(-\mu T_1^*) dT_1^*}{\int_1^{T_S^*} T_1^{*1/2} \exp(-\mu T_1^*) dT_1^*} = \frac{1 - T_G^{*1/2} \cdot \exp[\mu(1-T_G^*)] - \xi[\operatorname{erfc}(\mu T_G^*)^{1/2} - \operatorname{erfc}(\mu)^{1/2}]}{1 - T_S^{*1/2} \cdot \exp[\mu(1-T_S^*)] - \xi[\operatorname{erfc}(\mu T_S^*)^{1/2} - \operatorname{erfc}(\mu)^{1/2}]}, \tag{42}$$

where

$$\xi(\mu) = \frac{1}{2}\left(\frac{\pi}{\mu}\right)^{1/2} \cdot e^{\mu}.$$

With (16), (39), and (42) we obtain

$$x_{AB}(r^*) = x_{AB}(\infty) \exp\{\mu[1 - T_G^*(r^*)]\} + \left(\frac{1}{2} - \frac{\bar{\kappa}}{2\Delta\kappa}\right)(1 - \exp\{\mu[1 - T_G^*(r^*)]\}). \tag{43}$$

When we inset (43) into (15) we obtain an equation that permits calculation of the quantiy μ. Symbolically, this equation can be written in the form

$$\Phi(\mu)=\frac{\vartheta}{1+\vartheta} \tag{44}$$

with

$$\vartheta=\left[x_{AB}(\infty)\left(\frac{\kappa_{AB}(\infty)}{\kappa_B(\infty)}-1\right)\right]^{-1} \tag{45}$$

and

$$\Phi(\mu)=\exp[\mu(1-T_S^*)]-\frac{\mu T_S^*}{\varepsilon^*}\exp\left(\frac{\Delta E^*}{T_S^*}\right) \times\int_1^{T_S^*} T_1^{*1/2}\cdot\exp[\mu(1-T_1^*)]dT_1^*. \tag{46}$$

With the constant μ calculated from (44) to (46) we can determine the temperature $T_G^*(r^*)$ from the inverse function $r^*=r^*(T_G^*)$ in (42). Correspondingly, the concentration $x_{AB}^*(r^*)$ is obtained from (43) and it can be written in the form

$$x_{AB}^*(r^*)=(1+\vartheta)\exp[\mu(1-T_G^*)]-\vartheta. \tag{47}$$

The reaction rate becomes

$$W^*(T_S^*)=\frac{1}{T_S^*}\{(1+\vartheta)\exp[\mu(1-T_S^*)]-\vartheta\} \times\exp(-\Delta E^*/T_S^*). \tag{48}$$

Figure 8 shows an Arrhenius plot of the normalized reaction rate (48) for $\Delta E^*=90$, $\varepsilon^*=5\cdot10^6$ (note that the value of μ changes with ε^*) and for parameters $\vartheta=-2$, ∞, and $+2$. The figure shows that the influence of ϑ on W^* is very small.

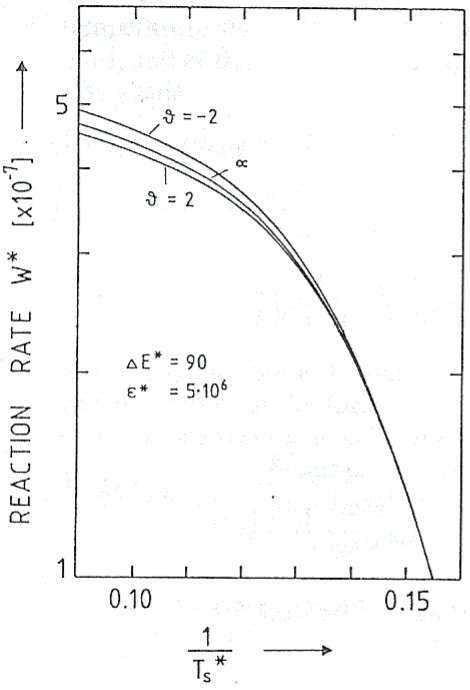

Fig. 8. Influence of concentration-dependent thermal conductivity, described by ϑ, see (45), on the reaction rate W^*. The other parameters were $\Delta E^*=90$ and $\varepsilon^*=5\times10^6$

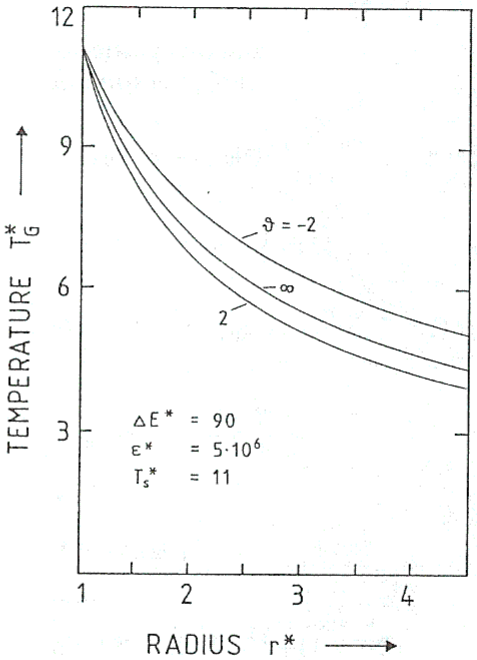

Fig. 9. Influence of concentration-dependent thermal conductivity on the spatial distribution of the gas-phase temperature, $T_G^*(r^*)$, for $\Delta E^*=90$, $\varepsilon^*=5\times10^6$, and $T_S^*=11$

The distribution of the normalized gas-phase temperature $T_G(r^*)$ is shown in Fig. 9 for $T_S^*=11$ and for values of $\vartheta=-2$, ∞, $+2$. The figure shows that the influence of ϑ becomes more pronounced with increasing distance r^*.

It should be noted that the concentration dependence of the thermal conductivity causes a coupling between the chemical and the thermal degrees of freedom of the system. Consider, for example, a constant temperature T_S at the surface of the reaction zone, and $\kappa_B(\infty)>\kappa_{AB}(\infty)$ which yields $\vartheta<0$. In this case the appearance of the reaction product B causes an increase of heat transport and, as a consequence, an increase in gas-phase temperature T_G (Fig. 9) and in concentration x_{AB}. The increase in gas-phase temperature, in turn, causes an increase in the molecular diffusion coefficient D_{AB} which, as a consequence, will increase the reaction rate (Fig. 8). Thus, with $\kappa_B(\infty)>\kappa_{AB}(\infty)$ a *positive* feedback between chemical and thermal degrees of freedom is observed. Correspondingly, if $\kappa_B<\kappa_{AB}$ ($\vartheta>0$) the feedback is *negative* and the reaction rate is decreased.

4. Thermal Diffusion

Up to now, we have considered mass transport by ordinary diffusion only. Because of the strong tempera-

ture gradients that occur in many cases of pyrolytic LCP, however, thermal diffusion can significantly influence gas-phase distributions of constituents and, as a consequence, surface reaction rates. This will be outlined in the subsequent calculations. Here, we will assume a reaction of the type (2) with $N_G \neq 0$. With the assumptions made (Sect. 1), we can approximate $x_B \approx 0$, and $x_G \approx 1 - x_{AB}$ (this includes the case $B \equiv G$ where $x_B \approx x_G$). We start again with the equation of continuity which can now be written in the form

$$\nabla \left[r^2 N(r) D_{AB}(r) \times \left(\nabla x_{AB}(r) + \frac{\alpha_t x_{AB}(r)\,[1 - x_{AB}(r)]}{T_G(r)} \cdot \nabla T_G(r) \right) \right] = 0 . \tag{49}$$

Here, α_t is the coefficient of thermal diffusion, whose sign depends on the relative size of masses m_{AB} and m_G according to

$$\alpha_t = \frac{m_{AB} - m_G}{m_{AB} + m_G} \alpha_0 , \tag{50}$$

where α_0 is assumed to be a constant. In general, the value of α_0 shows a weak dependence on concentration and temperature. With very high temperatures the α_0 may even change sign. For solving (49) we employ instead of (15) the boundary condition

$$D_{AB}(r_D) \left[\nabla x_{AB}(r) + \frac{\alpha_t x_{AB}(r)\,[1 - x_{AB}(r)]}{T_G(r)} \nabla T_G(r) \right]_{r_D} = k x_{AB}(r_D) . \tag{51}$$

The temperature distribution $T_G(r)$ is again calculated from (16) to (18). Here, we assume that the thermal conductivity κ is a constant. Furthermore, we assume temperature dependences of N as given by (6) with $q = 1$, and of D_{AB} as given by (25a). Then, integration of (49) yields

$$\nabla x_{AB}(r) - \alpha_t x_{AB}(r)\,[1 - x_{AB}(r)] \times \frac{\Delta T_S \cdot r_D}{T_G(\infty) \cdot r^2 + \Delta T_S \cdot r_D r} = \frac{C T_G^{n-1}(\infty)}{N(\infty) D_{AB}(\infty) r^2 [T_G(\infty) + \Delta T_S \cdot r_D / r]^{n-1}} , \tag{52}$$

where C is a constant of integration. Furthermore, (51) can be written in the form

$$\nabla x_{AB}(r)|_{r_D} = \frac{k x_{AB}(r_D)}{D_{AB}(\infty) \left(\frac{T_G(r_D)}{T_G(\infty)} \right)^n} + \alpha_t x_{AB}(r_D)\,[1 - x_{AB}(r_D)] \cdot \frac{\Delta T_S}{T_S \cdot r_D} . \tag{53}$$

If we determine $\nabla x_{AB}(r)$ at $r = r_D$ from (52), the comparison with (53) yields for the constant C

$$C = k x_{AB}(r_D) N(\infty) r_D^2 \left(\frac{T_G(\infty)}{T_S} \right) . \tag{54}$$

Inserting (54) into (52) and introducing the normalized quantities (10) to (12) yields

$$\nabla x_{AB}(r) - \alpha_t x_{AB}(r)\,[1 - x_{AB}(r)] \left(\frac{1}{\Delta T_S^*} + \frac{r_D}{r} \right)^{-1} \cdot \frac{r_D}{r^2} = W^* \varepsilon^* x_{AB}(\infty)\,[\Delta T_S^*]^{1-n} \cdot \left(\frac{1}{\Delta T_S^*} + \frac{r_D}{r} \right)^{1-n} \cdot \frac{r_D}{r^2} . \tag{55}$$

With the boundary condition (14), integration of (55) yields, for the simplest case, $n = 2$

$$x_{AB}(r) = \tfrac{1}{2} \left(1 + \beta \frac{\Psi + \beta + \Xi}{\Psi + \beta - \Xi} \right) \tag{56}$$

with

$$\Psi = 2 x_{AB}(r_D) - 1 \tag{57}$$

and

$$\Xi = (\Psi - \beta) \left[T_S^{*-1} + (1 - T_S^{*-1}) \cdot r_D / r \right]^{\alpha_t \beta} \tag{58}$$

and

$$\beta = \left(1 + \frac{4 W^* \varepsilon^* x_{AB}(\infty)}{\alpha_t \cdot \Delta T_S^*} \right)^{1/2} , \tag{59}$$

where W^* is the normalized reaction rate (11) which can be written as

$$W^* = \frac{x_{AB}(r_D)}{x_{AB}(\infty) T_S^*} \exp \left(- \frac{\Delta E^*}{T_S^*} \right) . \tag{60}$$

From (56) we obtain an implicit equation for the molar ratio x_{AB} at the surface of the reaction zone $r = r_D$, which can be written as

$$2\beta [x_{AB}(\infty) - x_{AB}(r_D)] = [\beta^2 - [2 x_{AB}(\infty) - 1] \cdot [2 x_{AB}(r_D) - 1]] \cdot \Gamma \tag{61}$$

with

$$\Gamma = \frac{1 - T_S^{*-\alpha_t \beta}}{1 + T_S^{*-\alpha_t \beta}} . \tag{62}$$

Subsequently, we consider solutions for $\beta^2 > 0$. With $\beta^2 < 0$ there are also real solutions which, however, are similar to those for $\beta^2 > 0$. With $\beta^2 < 0$ there are also *additional* solutions. These, however, contain singularities and are of no physical consequence.

Numerical solutions of (61) are plotted in Fig. 10 (full curves) and in Fig. 11 for $\Delta E^* = 90$ and $\varepsilon^* = 5 \times 10^6$.

Figure 10 shows the molar ratio $x_{AB}(r_D)$ as a function of the normalized substrate temperatures T_S^* with $x_{AB}(\infty) = 0.1$. The *full* curves refer to various

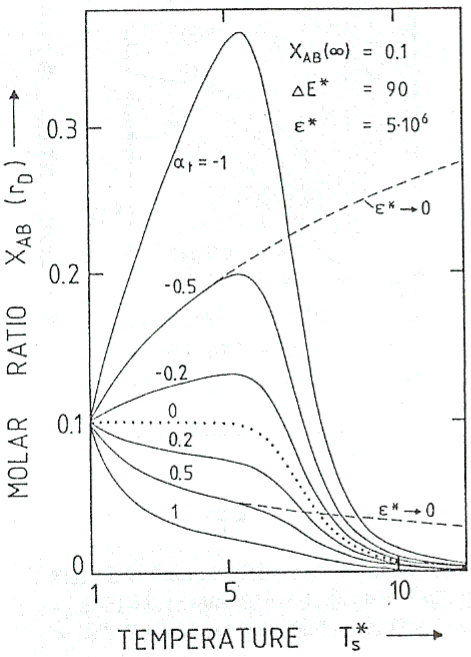

Fig. 10. Influence of thermal diffusion on the concentration of species AB at the surface of the reaction zone as a function of surface temperature for $\Delta E^*=90$, $\varepsilon^*=5\times10^6$, and $x_{AB}(\infty)=0.1$. *Full* curves refer to various values of α_t. *Dotted* curve: $\alpha_t\to0$. *Dashed* curves: $\varepsilon^*\to0$

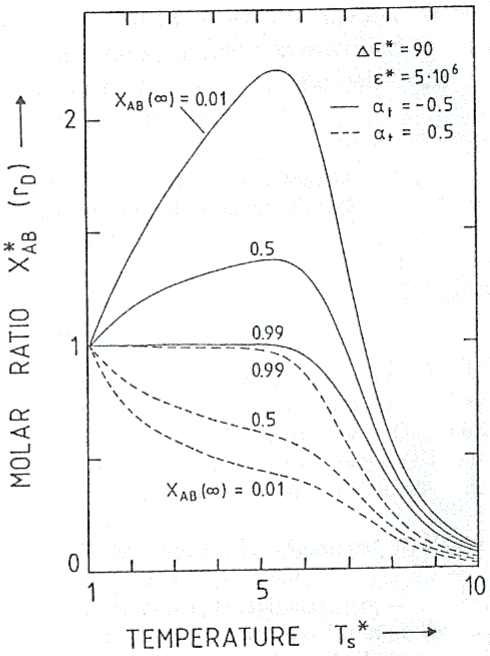

Fig. 11. Influence of thermal diffusion on the surface concentration $x^*_{AB}(r_D)$ as a function on surface temperature T_S^* for different values $x^*_{AB}(\infty)$. *Full* curves: $\alpha_t=-0.5$. *Dashed* curves: $\alpha_t=+0.5$

values of α_t. The dotted and dashed curves represent two limiting solutions of (61) which will be studied in the following.

Case 1: $\alpha_t\to0$.

In this limit we obtain from (59)

$$\beta^2\approx\frac{4W^*\varepsilon^*x_{AB}(\infty)}{\alpha_t\cdot\Delta T_S^*}\gg1 \tag{63}$$

and from (62)

$$\Gamma\approx\tfrac{1}{2}\alpha_t\beta\ln T_S^*\,. \tag{64}$$

With these approximations we obtain from (61)

$$x_{AB}(r_D)=x_{AB}(\infty)\left[1+\varepsilon^*\exp\left(-\frac{\Delta E^*}{T_S^*}\right)\times\frac{\ln T_S^*}{T_S^*(T_S^*-1)}\right]^{-1}. \tag{65}$$

This equation coincides with (30) for the case $n=2$ and $r^*=1$. The solution (65) is included in Fig. 10 by the *dotted* curve. Comparison with the full curves shows that the effect of thermal diffusion is most pronounced in the regime of medium to low substrate temperatures. At very high values of T_S^*, the ratio $x_{AB}(r_D)$ calculated from (61) can be well approximated by (65).

Case 2: $\varepsilon^*\to0$.

This limit characterizes the kinetically controlled regime. The spatial density of species, $N_{AB}(r)$, is determined only by the temperature distribution. With $\beta\approx1$ from (59), Eq. (61) yields

$$x_{AB}(r_D)=\left(1+\frac{1-x_{AB}(\infty)}{x_{AB}(\infty)}\,T_S^{*\alpha_t}\right)^{-1}. \tag{66}$$

This dependence is included in Fig. 10 by the *dashed* curves. These curves approximate the solutions (61) very well for values of $T_S^*\leqq5$ (compare dashed and full curves).

Figure 11 shows the normalized molar ratio $x^*_{AB}(r_D)$ as a function of T_S^* for various values of $x_{AB}(\infty)$. The *full* curves refer to $\alpha_t=-0.5$ while the *dashed* curves refer to $\alpha_t=+0.5$.

In both Figs. 10 and 11, thermal diffusion results in an increase in surface concentration $N_{AB}(r_D)$ if $\alpha_t<0$ and in a decrease of $N_{AB}(r_D)$ if $\alpha_t>0$. In other words, addition of a carrier gas G will increase the surface concentration of species AB if $m_G>m_{AB}$ and it will decrease it if $m_G<m_{AB}$. The latter situation is also possible with B≠G. Note that the effect of thermal diffusion becomes more pronounced with decreasing concentrations $x_{AB}(\infty)$ (Fig. 11).

We will now investigate the influence of thermal diffusion on the reaction rate (60). Here, the concentration $x_{AB}(r_D)$ must be calculated, for each temperature T_S^*, from the implicit equation (61). Figure 12 shows an Arrhenius plot of the rate W^* for $x_{AB}(\infty)=0.1$ and values of $\alpha_T=-1, 0$, and $+1$. The *full* curves refer to $\Delta E^*=90$, $\varepsilon^*=5\times10^6$, and the *dashed* curves to

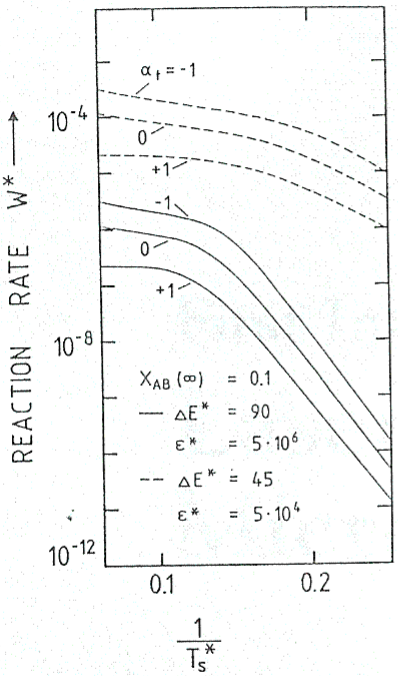

Fig. 12. Influence of thermal diffusion on the reaction rate W^* for $x_{AB}(\infty)=0.1$, and $\alpha_t=-1, 0, +1$. *Full* curves: $\Delta E^*=90$, $\varepsilon^*=5\times10^6$. *Dashed* curves: $\Delta E^*=45$, $\varepsilon^*=5\times10^4$

$\Delta E^*=45$, $\varepsilon^*=5\times10^4$. The figure reveals that thermal diffusion influences the kinetically controlled regime and the mass transport limited regime in a similar way. With respect to the case $\alpha_t=0$, the reaction rate is increased if $\alpha_t<0$, and decreased in the opposite case.

5. Conclusion

In both gas-phase and liquid-phase laser microchemical processing, consideration of temperature-dependent molecular diffusion increases calculated reaction rates within the mass transport limited region by up to about a factor of ten. On the other hand, both the temperature and the concentration-dependence of the thermal conductivity are of minor influence only. Thermal diffusion can significantly change reaction rates within both the mass-transport limited regime and the kinetically controlled regime. The sign of this change depends on the relative size of the masses of species involved.

Acknowledgement. We wish to thank the "Fonds zur Förderung der wissenschaftlichen Forschung in Österreich" for financial support.

References

1. D. Bäuerle: *Chemical Processing with Lasers*, Springer Ser. Mat. Sci. **1** (Springer, Berlin, Heidelberg 1986)
2. K. Piglmayer, J. Doppelbauer, D. Bäuerle: In *Laser Controlled Chemical Processing of Surfaces*, ed. by A.W. Johnson, D.J. Ehrlich, H.R. Schlossberg (North-Holland, New York 1984) p. 47
   P. Mogyorosi, K. Piglmayer, R. Kullmer, D. Bäuerle: Appl. Phys. A **45**, 293 (1988)
   R. Kullmer, D. Bäuerle: Appl. Phys. A **47**, 377 (1988)
   C.J. Chen: J. Vac. Sci. Technol. A **5**, 3386 (1987)
   D.J. Ehrlich, J.Y. Tsao: In *Laser Diagnostics and Photochemical Processing for Semiconductor Devices*, ed. by R.M. Osgood, S.R.J. Brueck, H.R. Schlossberg (North-Holland, New York 1983) p. 3
   K. Piglmayer, D. Bäuerle: Appl. Phys. B **48**, 453 (1989)
   F.V. Bunkin, N.A. Kirichenko, B.S. Luk'yanchuk: Bull. Acad. Sci. USSR, Phys. Ser. **45**, 1018 (1981)
3. V.G. Levich: *Physicochemical Hydrodynamics* (Prentice Hall, Englewood Cliffs, NJ 1962)
4. See, e.g., J.O. Hirschfelder, C.F. Curtiss, R.B. Bird: *Molecular Theory of Gases and Liquids*, (Wiley, New York 1964)
5. G. Leyendecker, H. Noll, D. Bäuerle, P. Geittner, H. Lydtin: J. Electrochem. Soc. **130**, 157 (1983)
   G. Leyendecker, D. Bäuerle, P. Geittner, H. Lydtin: Appl. Phys. Lett. **39**, 921 (1981)
6. G.G. Shafeev: Private communication